Electrodeposited Zn for Water-Repellent Coatings

Boyang Gao[1] and Kristin M. Poduska [1,2,*,z]

[1]*Department of Chemistry, Memorial University of Newfoundland, St. John's, NL A1B 3X7, Canada*
[2]*Department of Physics and Physical Oceanography, Memorial University of Newfoundland, St. John's, NL A1B 3X7 Canada*

We show that mildly alkaline electrolytes can be used to produce Zn coatings that improve the water repellent properties of stainless steel. Optimal Zn deposits were prepared under potentiostatic conditions from electrolytes that contained $ZnCl_2$, NH_4Cl, and a surfactant (polyethyleneimine). After deposition, the Zn electrodeposit was capped with stearic acid to prevent oxidation and to provide a lower surface energy. The capped electrodeposits display an impressive degree of water repellency, including extremely poor water droplet adhesion. We discuss the range of deposition parameters (electrolyte composition, pH, and applied potential) that produce the best water-repellent electrodeposits.

 [DOI: 10.1149/2.1141810jes]

Manuscript submitted May 8, 2018; revised manuscript received July 16, 2018. Published July 31, 2018.

Controlling the way that water wets a surface is a very popular research subject because it affects how durable the material will be against factors such as corrosion, ice accretion,[1,2] and fouling.[3] To reduce wetting of static water droplets, there are general guidelines and simple models that demonstrate this can be achieved with combinations of micron-scale and nanometer-scale surface roughness, in addition to a low surface energy.[4–6] This produces air pockets between water droplets and the surface, leading to superhydrophobicity with a very high apparent static contact angle. However, droplets that do not wet a superhydrophobic surface well can still adhere strongly, which makes them hard to remove even if the surface is tilted. It is still an open research question to model and predict exactly what structural characteristics prevent water droplets from adhering to a surface because this varies with droplet size, and it is also affected by topographic asperities on the surface.[7–9] For industrial structural materials such as stainless steel, reducing droplet adhesion is very desirable, but it is particularly difficult because of their innately high surface energy, multi-component chemical compositions, and complex surface shapes. Thus, it is a challenging and interesting research question to control both wettability and water adhesion on stainless steel.

Many groups have roughened stainless steel surfaces to improve their water repellent properties, using either removal strategies (such as chemical etching[10–13] and sandblasting[14–16]) or additive strategies (such as thermal evaporation,[17] sol-gel,[18] and electrodeposited layers[19–22]). Electrodeposits change the surface topography, and some studies have checked to see if this correlates with changes in static contact angles.[20–22] Adding surfactants to electrolytes is another strategy to control crystallite nucleation and growth. Such additives can alter the evolution and adsorption of hydrogen gas, and they can also passivate specific crystallite faces to alter crystallite morphologies. In the case of Zn, electrodeposition tends to produce dendritic crystallites where current distributions are not uniform, so additives are often beneficial.[23–26] Zn and Zn-alloy electrodeposition has been widely used as a corrosion protection barrier on steel.[19,20]

In this work, we demonstrate that a mildly alkaline electrolyte (pH=8) that contains a surfactant (polyethyleneimine, PEI) can be used to produce Zn electrodeposits that have very low adhesion for macroscopic water droplets. We discuss the range of deposition parameters (electrolyte composition, pH, applied potential, and coating procedures) that produce the best water-repellent surfaces.

Experimental

Electrodeposition.—Electrolytes contained 0.2 M $ZnCl_2$ (ACS grade, 97.0%, Caledon) and 3.5 M NH_4Cl (ACS grade, 99.5%, ACP) in ultrapure water (Barnstead, 18.2 MΩ·cm). We note that a large amount of white precipitate formed initially, but the solution cleared once the pH increased above 7.5 by adding NaOH (ACS grade, 97.0%, ACP). In this study, we used electrolytes with pH values between 7.5 and 8.5. After setting the desired pH, 100 ppm polyethyleneimine (PEI), a variable mass polymer with a repeat unit mass of 42.03 amu, was added as a surfactant.

Electrodeposits were prepared on high-strength, precipiation-hardened stainless steel (SAE 630/ 17-4, 1 mm thickness, McMaster-Carr) that is rich in Cr, Ni, and Cu. The 3 cm × 3 cm working electrodes were cleaned by sonication in ethanol (15 min, 95%, Commercial Alcohols, Inc.), then ultrapure water (15 min, 18.2 MΩ·cm, Barnstead), then drying in air at ambient temperature. The counter electrode was carbon felt (99.0%, Alfa Aesar), and all deposition potentials are reported relative to a saturated calomel (SCE) reference. Deposition was carried out at constant potential (−1.3 to −1.5 V vs. SCE) for 15 min at room temperature while stirring at 200 rpm. During the electrodeposition process, the current density typically decreased from −0.2 A/cm^2 to −0.15 A/cm^2. Afterwards, the sample was rinsed with ethanol and immediately immersed in an ethanol-based solution of 0.05 M stearic acid (95.0%, Sigma-Aldrich) for 5 min, then rinsed with ethanol and air-dried. For comparison, other samples were rinsed with ultrapure water (instead of ethanol) and allowed to air-dry before immersion in the stearic acid solution.

Characterization.—X-ray diffraction (XRD) data were collected with a Rigaku Ultima-IV (Cu Kα, λ = 1.54059 Å) over a range of 5-90° 2θ with 0.02° step size. Lattice constant refinements were facilitated with Jade software (Materials Data Inc.). Surfaces were imaged with an FEI MLA 650F scanning electron microscope (SEM) using secondary electron imaging (SEI) and backscattered electron (BSE) detection. Compositional data came from energy dispersive X-ray (EDX) detection on the same SEM. Surface roughness was assessed with profilometer scans (Alpha-Step D-120 Stylus Profiler) over 1 mm lengths with a 0.04 μm step size. Water droplet adhesion and static contact angles were assessed using droplets with 5 μL volume (Dataphysics OCA 15EC contact angle instrument).

Results and Discussion

We analyzed the structure, composition and crystallite morphologies of the resulting electrodeposits, as well as their water repellency properties. Representative XRD data (Figure 1) for electrodeposits

*Electrochemical Society Member.
[z]E-mail: kris@mun.ca

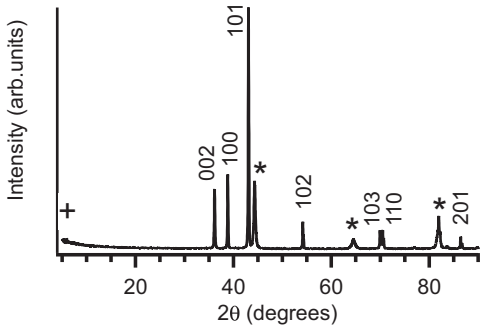

Figure 1. Representative XRD data for a Zn electrodeposit prepared at optimized deposition conditions (pH = 8, $E = -1.5$ V) and then coated with stearic acid. The *hkl* indexes correspond to the unit cell for hexagonal Zn (JCPDS 98-000-0482), asterisk (*) denotes peaks due to the stainless steel substrate, and plus (+) denotes a peak related to stearic acid.

with optimized water repellency (produced at pH = 8, $E = -1.5$ V) show eight peaks that are consistent with hexagonal Zn ($P6_3/mmc$ (194), JCPDS card 98-000-0482 with $a = 2.6650$ Å, $c = 4.9470$ Å).[27] The remainder of the peaks are associated with either the stainless steel substrate (*) or the stearic acid overcoat (+).

Even though XRD data indicate that the electrodeposits are pure Zn with no preferred orientation, SEM images show a mix of crystallite morphologies and orientations (Figure 3a). The majority of the deposit is composed of micron-scale blocky crystallites, and there are also needle-shaped and hexagonal plate habits interspersed over a scale of tens of micrometers.

Use of surfactant.—The crystallite morphology and substrate coverage of electrodeposited Zn has been widely studied, and the effects of additives – including complexing agents and surfactants – are widely reported. Because of its hexagonal crystal structure, the two most common crystal habits for Zn are plates or rods (needles).[28] As is typical for metal deposition, acidic pH values are commonly used for Zn electrodeposition. There are comparatively few reports that investigate Zn metal deposition from mildly alkaline electrolytes. Reports show that Zn electrodeposition based on ZnO and KOH as alkaline electrolytes also yields needle-shaped crystallites.[24,25] Using cetyltrimethylammonium bromide in the electrolyte surpresses dendritic growth and produces a higher density of small spherical crystallites.[25] Other additives such as PEI can change the morphology of dendrite tips from sharp to round.

In our experiments, Zn-based electrolytes without PEI surfactant had macroscopic variations in coverage and deposit color, and this was correlated with areas where hydrogen gas bubbles formed on the substrate during deposition. In areas of incomplete film coverage, water droplets adhered strongly to the surface and were easily pinned. SEM images show that the absence of PEI had a dramatic effect on the crystal habit of the Zn crystallites. Figure 2b shows blocky hexagonal crystals that are an order of magnitude larger than those produced from electrolytes that do contain PEI. In addition, there are gaps between

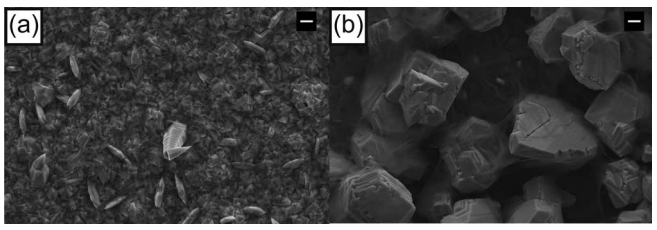

Figure 2. Representative SEM images of Zn electrodeposits (a) with PEI surfactant and (b) without surfactant. Scale bars for both images are 2 μm, and both samples were prepared at −1.5 V and pH = 8.

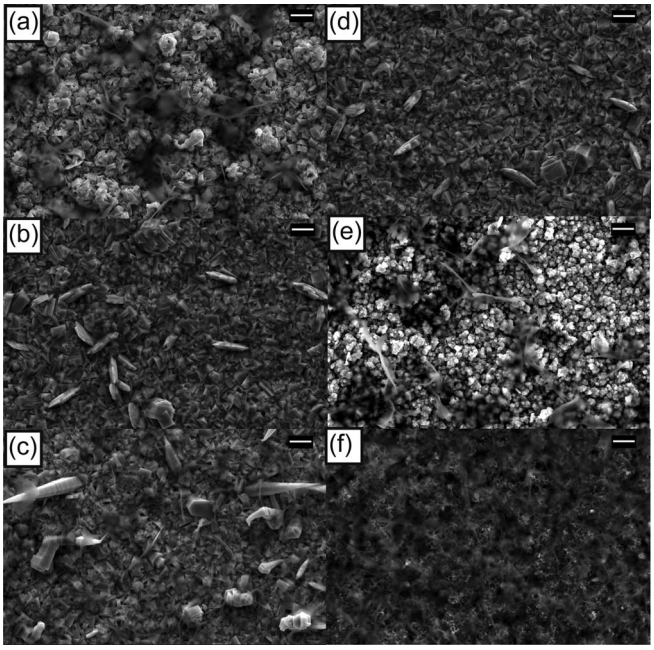

Figure 3. Representative SEM images of Zn electrodeposits. At constant deposition potential (−1.5 V), more alkaline pH values ((a) at 7.5) affect size and shape relative to more neutral pH ((b) at 8.0 and (c) at 8.5). Keeping the same pH value (8.0) and making the deposition potential less negative leads to more uniform crystallite sizes and shapes ((d) at −1.5 V, (e) at −1.4 V, (f) at −1.3 V). Scale bars for all SEM images are 2 μm.

individual crystallites that are tens of micrometers in size. For these reasons, we opted to use PEI in all of our electrolytes. We note that there was no evidence of PEI incorporation into the electrodeposits, based on XRD data.

Variation of pH and deposition potential.—In general, Pourbaix diagrams are a helpful tool for optimizing electrodeposition conditions because they identify the pH and potential regions that will give a desired electrodeposit composition. We based our electrolyte on calculated Pourbaix diagrams for the Zn-NH_4Cl-NH_3-H_2O system,[26] but with the addition of PEI surfactant. The useful pH and potential range we found for Zn deposition was consistent with the calculated Pourbaix diagrams.

In ammonium- and chloride-containing electrolytes, the kinds of Zn-based solution complexes vary considerably as a function of pH, especially near neutral pH.[26] $ZnNH_3Cl_3^-$ dominates when pH is between 7 to 7.4, while $Zn(NH_3)_3Cl^+$ forms when the pH ranges from 7.4 to 7.8. When pH sits between 7.8 and 12.5, $Zn(NH_3)_4^{2+}$ is the primary complex. In our experiments, white precipitates formed when the pH value was near 7, but disappeared once the pH increased above 7.5. As the alkalinity of the electrolyte increased, more negative deposition potentials were required to trigger Zn deposition, which caused more hydrogen gas bubbles to appear on the sample during deposition, resulting in incomplete deposit coverage. Therefore, we determined that mildly alkaline electrolytes (7.5-8.5) were optimal for our purposes. Adjusting the electrolyte pH over this small range had an effect on the electrodeposit topography. As shown in Figure 3a-3c, there are more large needle-shaped crystallites at higher pH values, when using the same deposition potential ($E = -1.5$ V).

We also investigated the effects of changing deposition potential between −1.0 V to −1.5 V, in steps of 0.1 V. At deposition potentials more positive than −1.3 V, no deposit formed. At −1.3 V, the Zn crystallites are sub-μm particles without clear facets. At −1.4 V, there are μm-sized overlapping hexagonal crystallites. At −1.5 V, needles and large blocky agglomerates appear at the expense of the overlapping hexagonal crystallites. Therefore, more negative deposition potentials

give rise to larger sizes and more variety in the Zn electrodeposit morphologies. Representative SEM images over the range of potential and pH conditions are shown in Figures 3d-3f.

Given that there are so many changes in the surface topography of the electrodeposit induced by different electrolyte pH and deposition potentials, it is worthy of note that there was a correlation between the electrodeposition conditions and the resulting water repellency. In all cases described above (pH between 7.5 and 8.5, E between −1.3 V and −1.5 V), there are significant portions of the 9 cm^2 sample on which water droplets do not adhere. The best deposition conditions were pH values of 8.0-8.5 using a deposition potential of −1.5 V. With these optimized parameters, the entire 9 cm^2 surface was routinely free of droplet pinning sites, except for the few mm around the deposit edges. We note that, for these experiments, the distance between the WE and CE was 4 cm, and this yielded a current density near 0.033 A/cm^{-2}. A closer electrode spacing (3 cm), increased the current density (0.045 A/cm^{-2}, but did not show an appreciable change in droplet pinning.

Protection from water and oxidation.—A stearic acid overlayer plays a key role in preserving the integrity of the Zn electrodeposits. As mentioned in the Experimental description above, the electrodeposit must be rinsed with ethanol and immersed in the stearic acid immediately. When this capping layer is added, the electrodeposits retain their poor water-adhesion behaviors for many months. This is not surprising, since stearic acid is known to be an effective lubricant for stainless steel.[29,30]

If the electrodeposit is rinsed with water, the sample must dry before it comes in contact with the water-insoluble stearic acid solution to prevent precipitation. However, during that drying process, Zn reacts with moisture and electrolyte salts in a way that destroys the poor water-adhesion properties of the deposit, even after coating with stearic acid to lower the surface energy. On these stearic-acid-coated water-rinsed samples, water droplets adhere easily all over the surface. Furthermore, the apparent static contact angles vary greatly, ranging from 90° to 135°, with the lowest contact angles occurring in the impurity-phase-rich portion of the deposit.

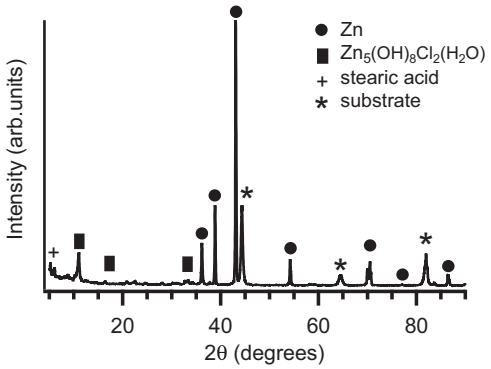

Figure 4. Representative XRD data for a water-rinsed electrodeposit that shows evidence of $Zn_5(OH)_8Cl_2(H_2O)$ (JCPDS 98-000-7203) in addition to metallic Zn (JCPDS 98-000-0482).[27] The asterisk (*) denotes peaks due to the stainless steel substrate, and plus (+) denotes a peak related to stearic acid.

XRD data (Figure 4) show that the composition of the water-rinsed electrodeposits includes both Zn metal and $Zn_5(OH)_8Cl_2(H_2O)$,

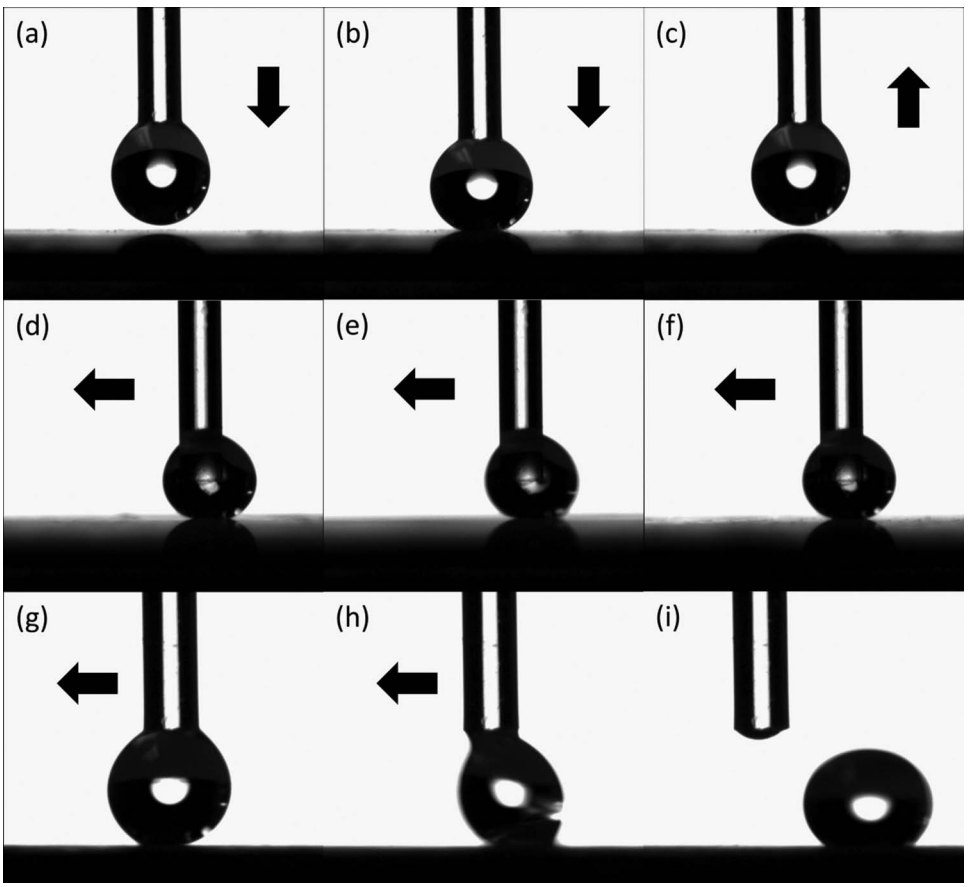

Figure 5. Representative image sequences of water droplets being moved across electrodeposit surfaces. For (a-c), a water droplet at the end of a syringe is brought into contact and then lifted from the electrodeposit. For (d-f), a similar droplet was slid across the surface without sticking. For (g-i), a sliding droplet was pinned to an inhomogeneity on the electodeposit and was detached from the syringe needle.

(simonkolleite, JCPDS card: 98-000-7203, with $a = 6.3412$ Å, $c = 23.6460$ Å). This composition is consistent with EDX data (not shown), which confirmed the presence of Cl and additional O in the deposit. Profilometer data (Figure 6) indicates that this hydroxide product alters the topography of the electrodeposit by introducing features that are ~10 μm tall, and these tall features do not develop uniformly across the sample. This is consistent with inspection by eye, which shows mm-cm sized regions where the dark gray electrodeposit turns white.

The formation of this impurity phase is not surprising. Based on the thermodynamics of Zn speciation calculated by others,[26] zinc hydroxychloride precipitates appear near neutral pH for low concentrations of Cl^- or NH_3 ($\leq$1 M) or for very high Zn concentrations ($\geq$1.93 M). By going to more alkaline conditions, $Zn(NH_3)_4^{2+}$ becomes the dominant species in the electrolyte, which increases Zn^{2+} solubility and reduces hydroxide precipitation. This is consistent with the precipitate formation and disappearance that we observed when our electrolyte pH was adjusted from slightly acidic levels to a slightly alkaline range. However, we note that this precipitation behavior occurred even though we used a low Zn concentration (0.2 M Zn^{2+}) and high Cl^- and NH_3 concentrations ($\geq$3.5 M).

Interactions with water droplets.—Upon visual inspection of the optimized stearic-acid-coated electrodeposits, it was immediately obvious that there was virtually no adhesion of macroscopic water droplets over large (cm-scale) areas. Water that squirted from a squeeze bottle or a syringe onto the surface bounced off and did not stick, except on the very edges of the substrate. Images from a more controlled version of this experiment are shown in Figure 5. In the top row, a needle was used to bring a 5 μL water droplet down to touch the electrodeposit surface. When the needle lifted, the water droplet remained on the needle instead of sticking to the electrodeposit. A similar response occurs when a droplet was dragged across the surface, as shown in the middle row of Figure 5. Along most parts of the surface, the droplet remained affixed to the needle while being dragged across cm-scale distances. However, there were a few places on each 9 cm^2 surface where the droplet was pulled off the needle and adhered to the surface; an example of this is shown in the bottom row of Figure 5. It is only at these anomalous "sticky" spots where the static contact angle could be measured, with typical values of 140 ± 5°. (For comparison, the apparent static contact angle of water on the bare stainless steel is 74 ± 3°.) Over the vast majority of the electrodeposit area, poor droplet adhesion prevented measurement of a static contact angle because the droplet rolled off the sample.

Although it is hard to design surfaces with poor water droplet adhesion a priori, empirical evidence in the literature shows that such surfaces have a synergy of micrometer-scale roughness and low surface energy.[2,3,6] In the case of our electrodeposits, SEM images indicate that the surface topography was dramatically changed after electrodeposition. However, the resulting surface topographies are very intricate and are not easily quantified accurately across all relevant length-scales (nanometer to micrometer) with scanning probe methods. Profilometer data (Figure 6a) indicates that, over a 1 mm length scale, the root-mean-square (rms) roughness of the electrodeposit is 2.0 ± 0.9 μm, which is higher than the roughness of the bare stainless steel (1.0 ± 0.3 μm). Based on this correlation between higher rms roughness and better water repellency, it is tempting to conclude that an rms roughness value difference is sufficient to explain the variations in water repellency between our optimized and less-perfect samples. However, this simple correlation is misleading because our coatings have roughnesses that vary across different length scales. To illustrate this point more clearly, Figure 6b shows four scans on different regions of an oxidized electrodeposit. The rms roughness values of these four scans are (in units of μm): 2 ± 1, 4 ± 1, 5 ± 2, 8 ± 4. This shows that oxidized samples have roughness heterogeneity at length scales longer than 1 mm that are not captured clearly in a single rms roughness value. Recent work by others[31] has shown that fractal models of roughness across many length scales can, in principle, be correlated with surface wettability. It would be an interesting future study, going beyond the scope of the present work, to explore whether roughness across many length scales could also be correlated with liquid droplet adhesion and water repellency as well.

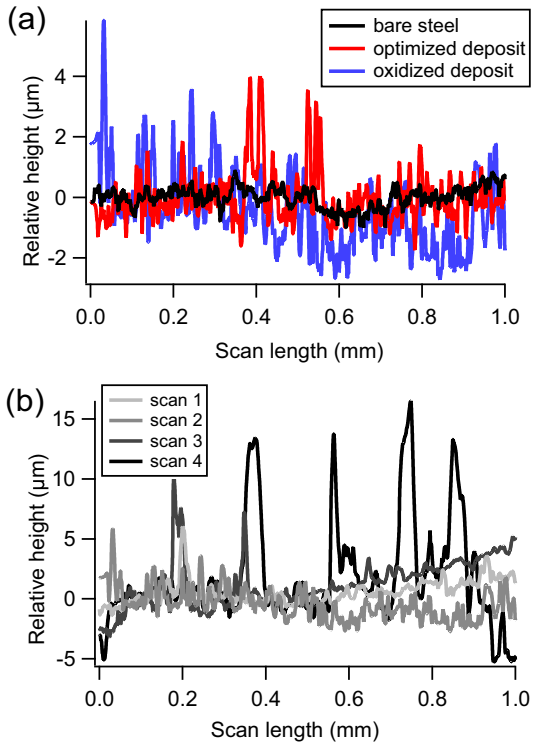

Figure 6. Representative profilometer scans of (a) bare stainless steel (black), ethanol-rinsed electrodeposit (red), and water-rinsed electrodeposit (blue). Corresponding root-mean-square (rms) roughness values are (in units of μm): 1.0 ± 0.3, 2.0 ± 0.9, and 4.0 ± 0.8. In (b), four different scans of a single water-rinsed electrodeposit are compared. Corresponding root-mean-square (rms) roughness values are (in units of μm): 2 ± 1, 4 ± 1, 5 ± 2, and 8 ± 4.

Discussion of water adhesion on electrodeposits.—It is worthy to note that not all hydrophobic surfaces show poor water droplet adhesion. In general, hydrophobic surfaces are defined to be those on which water droplets have static contact angles greater than 90°. However, there is often quite a range of contact angles that are measured because droplets can be pinned by chemical or topological heterogeneities on the surface. A more complete description of surface wettability involves measuring the contact angles of dynamic droplets, by adding water volume to the droplet until the water/solid contact line advances (to assess the maximum advancing contact angle) and then removing water volume from the droplet until the water/solid contact line recedes (to assess the minimum receding contact angle).[7] Others have used these advancing and receding angles to describe water repellency in terms of the force required to start a drop sliding on a surface (shear hydrophobicity) or the force required to remove a hanging drop from a surface (tensile hydrophobicity).[6]

In the case of our electrodeposits, macroscopic water droplets (5 μL with 2 mm diameter) never adhered to most parts of the surface, making it impossible to do standard static and dynamic contact angle measurements. This suggests that, in those regions of the electrodeposit, the force needed to remove a droplet from the surface, in either tensile mode (hanging droplet, Figures 5a-5c)s or shear mode (droplet sliding, Figures 5c-5f) is exceedingly low.

Even though there exist models to quantify droplet adhesion on surfaces, there are no definitive strategies for predicting (or explaining) which combinations of surface features will produce a water-repellent

surface.[7] In this way, any recipes for producing water-repellent surfaces offer opportunities to augment our phenomenological understanding. There are some reports of water-repellent electrodeposits, which tend to involve micrometer-scale roughened surface topographies capped with organic coatings. For example, Cu-based electrodeposits with complex multi-scale surface features, when coated with stearic acid, repel 10 μL water droplets.[31] Zn-Ni electrodeposits, etched with NaOH to change the surface roughness and then coated with myristic acid, repel water droplets that have volumes of 10s of μL.[21] Water droplets with μL volumes also slide easily off anodically produced CuO needles with fluoroalkyl-silane surface modification.[32] This suggests that many different kinds of surface topographies and chemistries can be effective for water-repellency, and that electrodeposition can play a useful role.

Conclusions

We show that Zn electrodeposits can improve the water repellent properties of stainless steel by reducing water droplet adhesion in a dramatic fashion. There is a relatively narrow range of electrolyte pH and deposition potentials that will yield optimized deposits. This is consistent with Pourbaix diagrams, calculated by others, that are based on speciation and solubility trends for different Zn(II) complexes that form in the presence of chloride and ammonia. Capping the Zn electrodeposits with stearic acid is essential to prevent oxidation and to provide a lower surface energy for water repellency.

Acknowledgment

Financial support for this research was provided by Petroleum Research Newfoundland & Labrador (PRNL) Canada with grant C15-03 and the Department of Tourism, Culture, Industry and Innovation of Newfoundland & Labrador (TCII) Canada with grant 5404.1891.102.

ORCID

Kristin M. Poduska https://orcid.org/0000-0003-4495-0668

References

1. A. J. Meuler, G. H. McKinley, and R. E. Cohen, *ACS Nano*, **12**, 7048 (2010).
2. M. J. Kreder, J. Alvarenga, P. Kim, and J. Aizenberg, *Nature Rev.*, **1**, 1 (2016).
3. R. Fürstner, W. Barthlott, C. Neinhuis, and P. Walzel, *Langmuir*, **21**, 956 (2005).
4. R. N. Wenzel, *Ind. Eng. Chem.*, **28**, 988 (1936).
5. A. Marmur, *Langmuir*, **24**, 7573 (2008).
6. L. Gao and T. J. McCarthy, *Langmuir*, **25**, 14105 (2009).
7. Y. V. Kalinin, V. Berejnov, and R. E. Thorne, *Langmuir*, **25**, 5391 (2009).
8. E. Bormashenko, *Adv. Colloid Interface Sci.*, **222**, 92 (2015).
9. W.-Z. Yuan and L.-Z. Zhang, *Langmuir*, **33**, 820 (2017).
10. P. Nageswara Rao and D. Kunzru, *J. Micromech. Microeng.*, **17** (2007).
11. S. S. Latthe, P. Sudhagar, A. Devadoss, A. M. Kumar, S. Liu, C. Terashima, K. Nakata, and A. Fujishima, *J. Mater. Chem. A*, **3**, 14263 (2015).
12. H. Zhang, J. Yang, B. Chen, C. Liu, M. Zhang, and C. Li, *Appl. Surf. Sci.*, **359**, 905 (2015).
13. L. Li, V. Breedveld, and D. W. Hess, *ACS. Appl. Mater. Inter.*, **4**, 4549 (2012).
14. D. J. Varacalle Jr., D. P. Guillen, D. M. Deason, W. Rhodaberger, and E. Sampson, *J. Thermal Spray Technol.*, **15**, 348 (2006).
15. S. Yu, X. Wang, W. Wang, Q. Yao, J. Xu, and W. Xiong, *Appl. Surf. Sci.*, **271**, 149 (2013).
16. F. Montes Ruiz-Cabello, A. Amirfazli, M. Cabrerizo-Vílchez, and M. Rodríguez-Valverde, *RSC Advances*, **6**, 71970 (2016).
17. S. Beckford and M. Zou, *Thin Solid Films*, **520**, 1520 (2011).
18. X. Feng, L. Feng, M. Jin, J. Zhai, L. Jiang, and D. Zhu, *J. Am. Chem. Soc.*, **126**, 62 (2004).
19. F. Berger, J. Delhalle, and Z. Mekhalif, *Electrochimica Acta*, **54**, 6464 (2009).
20. X. Zhang, J. Liang, B. Liu, and Z. Peng, *Colloid. Surface. A.*, **454**, 113 (2014).
21. T. Xiang, M. Zhang, C. Li, S. Zheng, S. Ding, J. Wang, C. Dong, and L. Yang, *J. Alloy. Compd.*, **704**, 170 (2017).
22. Y. Fan, Y. He, P. Luo, X. Chen, and B. Liu, *Appl. Surf. Sci.*, **368**, 435 (2016).
23. C. Cachet and R. Wiart, *Electrochim. Acta.*, **44**, 4743 (1999).
24. S. J. Banik and R. Akolkar, *Electrochim. Acta.*, **179**, 475 (2015).
25. K. Miyazaki, A. Nakata, Y. S. Lee, T. Fukutsuka, and T. Abe, *J. Appl. Electrochem.*, **46**, 1067 (2016).
26. J. Vazquez-Arenas, F. Sosa-Rodriguez, I. Lazaro, and R. Cruz, *Electrochim. Acta.*, **79**, 109 (2012).
27. *Joint Commission on Powder Diffraction Standards, International Centre for Diffraction Data, http://www.icdd.com* **2003**.
28. Y. H. Chen, H. W. Yeh, N. C. Lo, C. W. Chiu, I. W. Sun, and P. Y. Chen, *Electrochim. Acta.*, **227**, 185 (2017).
29. M. Ruths, S. Lundgren, K. Danerlo, and K. Persson, *Langmuir*, **24**, 1509 (2008).
30. M. Ratoi, V. Anghel, C. Bovington, and H. Spikes, *Tribol. Int.*, **33**, 241 (2000).
31. R. Jain and R. Pitchumani, *Langmuir*, **33**, 7187 (2017).
32. F. Xiao, S. Yuan, B. Liang, G. Li, S. O. Pehkonen, and T. Zhang, *J. Mater. Chem. A*, **3**, 4374 (2015).